DOI: 10.1002/ejic.200900309

Resonance Raman Studies of Bis(terpyridine)ruthenium(II) Amino Acid Esters and Diesters

Katja Heinze,*[a] Klaus Hempel,[b] Stefanie Tschierlei,[c] Michael Schmitt,[c] Jürgen Popp,[c] and Sven Rau[d]

Keywords: Charge transfer / Density functional calculations / Raman spectroscopy / Ruthenium / Terpyridine

Resonance Raman (rR) spectroscopy in combination with DFT calculations was used to elucidate the nature of the ^{1}metal-to-ligand charge-transfer states (^{1}MLCT) of ester derivatives of homo- and heteroleptic bis(terpyridine)ruthenium(II) complexes $[Ru^{II}(tpy–COOC_2H_5)(tpy–R)](PF_6)_2$ with R = NH_2 (**1a**), R = $COOC_2H_5$ (**1b**) and R = $NHCOCH_3$ (**1c**). The rR spectra provide evidence that the ^{1}MLCT states of **1b** and **1c** are well described by the expected $^1[(\text{“}t_{2g}\text{”})^5\{\pi^*(tpy–COOC_2H_5)\}^1]$ electron configuration, while the ^{1}MLCT state of the donor/acceptor-substituted complex **1a** also involves the amine-substituted terpyridine ligand. The excited state of **1a** can be described by a $^1[\{d_{yz}/\pi(tpy–NH_2)\}^1\{\pi^*(tpy–COOC_2H_5)\}^1]$ electron configuration with ligand-to-ligand charge-transfer (^{1}LLCT) character. The mixed MLCT/LLCT character of the singlet excited state of **1a** is characterized by a low-energy absorption maximum (λ_{max} = 500 nm). The π-donor character of the tpy–NH_2 ligand is also corroborated by DFT calculations on model compounds (small HOMO/LUMO gap, short C–N bond, longer Ru–N bond). The emitting triplet state features a low-energy emission maximum (λ_{max} = 744 nm) as well as a longer lifetime of the emitting state (τ = 33.7 ns) at room temperature in acetonitrile as compared to the data of **1b** and **1c**.

Introduction

Over the last decades polypyridyl-ruthenium complexes have attracted particular attention due to their interesting and potentially useful photophysical properties.[1,2] The parent complex $[Ru(bpy)_3]^{2+}$ possesses a long-lived emissive triplet ^{3}MLCT state at room temperature (bpy = 2,2′-bipyridine) which is important for applications in practical devices which rely on solar energy such as dye sensitized solar cells (DSSCs).[3–6] However, $[Ru(bpy)_3]^{2+}$ has only a weak absorbance in the red part of the solar spectrum ($\lambda_{max} \approx$ 450 nm)[7] so intense research efforts have been devoted to the extension of the absorption window of such complexes.[8–11] $[Ru(tpy)_2]^{2+}$ complexes feature a bathochromically shifted absorption band around $\lambda_{max} \approx$ 500 nm (tpy = 2,2′;6′,2′′-terpyridine). However, these complexes are usually almost non-emissive at room temperature in fluid medium. In fact, the parent $[Ru(tpy)_2]^{2+}$ complex has a very short-lived excited ^{3}MLCT state (250 ps in H_2O and 120 ps in CH_3CN/H_2O, 3:2) and a very low quantum yield of emission at room temperature in fluid medium.[12] One possibility to enhance the excited state properties of $[Ru(tpy)_2]^{2+}$ complexes is to entrap the complex in porous matrices (e.g. zeolites[13]) while a different approach is based on substitution of the terpyridine ligands on the 4′ positions with electron-donating or -withdrawing groups.[11,14,15,16,17] For example, $[Ru(tpy)(tpy–COOC_2H_5)]^{2+}$ emits at λ_{max} = 667 nm with a quantum yield of $\phi = 2.7 \times 10^{-4}$ and τ = 32 ns at 298 K in acetonitrile.[16]

Besides these interesting photochemical properties heteroleptic $[Ru(tpy–R)(tpy–R')]^{2+}$ complexes with substituents in 4′ position are not stereogenic in contrast to the trischelate $[Ru(bpy)_3]^{2+}$ complexes. This feature is very important for the implementation of photoredoxactive units into multinuclear assemblies as it facilitates synthesis and purification and still offers the possibility for functionalisation. This becomes evident in bipyridine-ruthenium(II) complexes where the simultaneous presence of donor- and acceptor-substituted bipyridines bpy–R and bpy–R′ – essential for efficient vectorial charge-separation processes in excited complexes – results in complicated mixtures of complexes with different charge-separation properties. A well-defined separation between donor and acceptor substitu-

[a] Institute of Inorganic Chemistry and Analytical Chemistry, Johannes Gutenberg-University of Mainz, Duesbergweg 10-14, 55128 Mainz, Germany
Fax: +49-6131-39-27277
E-mail: katja.heinze@uni-mainz.de
[b] Department of Inorganic Chemistry, Ruprecht Karls-University of Heidelberg, Im Neuenheimer Feld 270, 69120 Heidelberg, Germany
[c] Institute of Physical Chemistry, Friedrich Schiller-University of Jena, Helmholtzweg 4, 07743 Jena, Germany
[d] Department of Chemistry and Pharmacy, Friedrich Alexander-University of Erlangen-Nürnberg, Egerlandstraße 1, 91058 Erlangen, Germany
Supporting information for this article is available on the WWW under http://dx.doi.org/10.1002/ejic.200900309.

ents (R/R′) is easily achieved in heteroleptic [Ru(tpy–R)-(tpy–R′)]$^{2+}$ complexes with R and R′ located at the 4′ positions of the terpyridine ligands.[14]

Recently, we have introduced a heteroleptic [Ru(tpy–R)-(tpy–R′)]$^{2+}$ complex with R = COOH and R′ = NH_2 giving the metallo amino acid **A** which places the metal centre in between the functional groups (Scheme 1).[18] This feature is exclusive for **A** in contrast to other ruthenium containing amino acids reported so far (**B**,[19] **C**,[20] **D**,[21] **E**[22]) with ruthenium located at the side-chain (Scheme 1). Such amino acid building blocks allow constructing and synthesising metallo peptides by solid-phase synthesis techniques.[23] Incorporation of ruthenium in the main chain of a peptide as opposed to peptides modified at the side chain should give rise to enhanced electronic communication between building blocks.

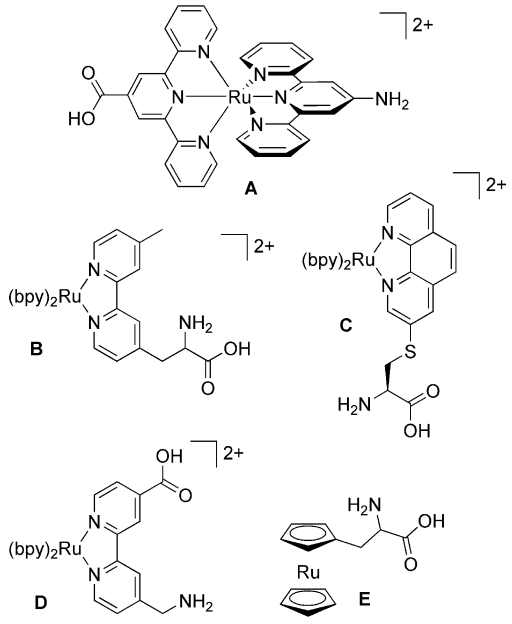

Scheme 1. Ruthenium(II)-containing artificial amino acids **A**–**E** (bpy = 2,2′-bipyridine).[18–22]

Indeed, energy transfer processes have been observed in amide-linked dyads composed of **A** and organic chromophores, e.g. coumarins.[23b] Furthermore ferrocene derivatives have been successfully coupled to the artificial amino acid **A** via amide bonds either at the *N*- or at the *C*-terminus and photo-induced electron transfer (PET) has been observed provided that the redox potential of the ferrocene unit is energetically below the excited state redox potential of the ruthenium moiety.[18]

In order to get a deeper insight into the first events of electronic excitation in derivatives of amino acid **A** we now have performed a resonance Raman (rR[24]) study of the ethyl ester derivative of **A** (**1a**). Raman transitions that are associated with structural distortions upon photoexcitation to the excited state are enhanced. In the present investigation the ester **1a** is favoured over the acid **A** as the ground state properties of the free acid **A** are naturally pH-dependent and the emitting excited state shows a complicated decay characteristic (which is probably influenced by hydrogen bonding and/or proton transfer).[18,23] For comparison reasons the diester **1b**[25] and the acetyl derivative **1c** were also prepared and investigated (Scheme 2). Recently, for heteroleptic poly(bipyridine)-[26,27] and phenanthroline/tetraazatetrapyridopentacene-ruthenium(II) complexes[28] resonance-Raman studies have demonstrated that rR is a useful method to investigate the nature of the inital ^{1}MLCT state of heteroleptic ruthenium polypyridine complexes relevant for applications in DSSCs[29] and other artificial photosynthetic systems.[30]

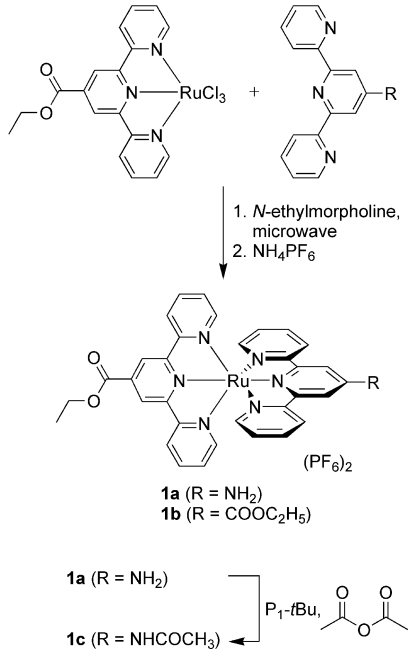

Scheme 2. Synthesis of complexes **1a**–**1c**.

Results and Discussion

Ruthenium containing amino acid ester **1a** was prepared by reaction of $RuCl_3$(tpy–$COOC_2H_5$) with tpy–NH_2 in a microwave synthesiser at 120 °C in ethanol[18] while diester **1b** was prepared analogously using tpy–$COOC_2H_5$ instead of tpy–NH_2 (see Scheme 2).[25] The acetyl protected derivative **1c** was synthesized from **1a** by the action of acetic anhydride in the presence of the phosphazene base P_1-*t*Bu [P_1-*t*Bu = *tert*-butylimino-tris(dimethylamino)phosphorane] in 94% isolated yield (Scheme 2).

The Ru^{II}/Ru^{III} redox potentials of **1a**–**1c** were measured in CH_3CN/nBu_4NPF_6 and the data are compiled in Table 1.[18,25] Amine complex **1a** is the most easily oxidized while **1b** is the most difficult oxidized complex in this series pointing to an increasing HOMO energy from **1b** to **1c** to **1a**.

All three complexes **1a**–**1c** display an asymmetric ^{1}MLCT absorption band $^1[(\text{“}t_{2g}\text{”})^6] \rightarrow {}^1[(\text{“}t_{2g}\text{”})^5(\pi^*)^1]$ in the visible spectral region which is characteristic for [Ru-

Table 1. Photophysical and electrochemical data of complexes **1a**–**1c** in CH_3CN at room temperature.

	MLCT absorption λ_{max} (ε) / nm ($M^{-1}cm^{-1}$)	Emission λ_{max} / nm	ϕ	τ / ns	$E_{1/2}$ / V vs. SCE (Ru^{II}/Ru^{III})
1a	500 (19220)	744	1.8×10^{-3}	33.7	1.08[18]
1b	489 (23410)	652	1.6×10^{-3}	20.5	1.42[25]
1c	491 (21600)	690	1.6×10^{-3}	21.7	1.25

$(tpy)_2]^{2+}$ complexes (Table 1, Figure 1). At the low energy side shoulders are observed which can be assigned to direct excitations into ^{3}MLCT states $^1[(\text{“}t_{2g}\text{”})^6] \rightarrow {}^3[(\text{“}t_{2g}\text{”})^5(\pi^*)^1]$ which is allowed due to spin-orbit coupling.[33] In this series the heteroleptic donor/acceptor-substituted complex **1a** absorbs at the lowest energy (λ_{max} = 500 nm) while complexes **1b** and **1c** absorb at $\lambda_{max} \approx$ 490 nm (Table 1, Figure 1). A single ester moiety in $[Ru(tpy)(tpy–COOC_2H_5)]^{2+}$ shifts the absorption maximum to λ_{max} = 485 nm[16] as compared to that of the parent complex $[Ru(tpy)_2]^{2+}$ (λ_{max} = 476 nm[34]).

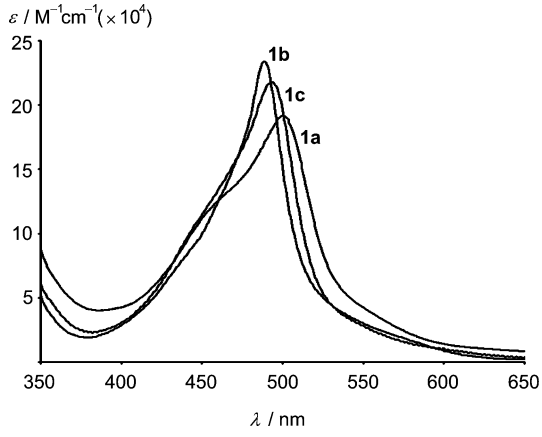

Figure 1. UV/Vis absorption spectra of **1a**–**1c** in CH_3CN at room temperature.

The emission spectra of **1a**–**1c** in fluid solution display the same trend as the absorption spectra with the emitting ^{3}MLCT state of **1a** being located at the lowest energy in this series (Table 1, Figures 1 and 2). Also the excited state lifetime τ measured for **1a** is significantly higher than those of **1b** and **1c** (Table 1).

The fact that the push-pull-substituted complex **1a** displays the most bathochromically shifted absorption and emission maxima agrees well with, for example, the trend observed in the donor/acceptor-substituted bipyridine-ruthenium(II) complexes $[Ru(tbbpy)_{3-n}(dmcb)_n]^{2+}$ (tbbp = 4,4′-di-*tert*-butyl-2,2′-bipyridine; dmcb = 4,4′-dimethoxycarbonyl-2,2′-bipyridine).[26] These heteroleptic complexes with n = 1, 2 display two absorption maxima with the lowest energy absorption maximum being assigned to a $^1[(\text{“}t_{2g}\text{”})^6] \rightarrow {}^1[(\text{“}t_{2g}\text{”})^5\{\pi^*(dmcb)\}^1]$ transition on the basis of resonance Raman spectroscopy.[26]

In order to obtain further insight into the location of the ^{1}MLCT excited state of **1a**–**1c** we employed resonance Raman spectroscopy. Resonance Raman spectra of **1a**–**1c** were measured in CH_3CN with an excitation at λ_{exc} = 488 nm (provided by an argon ion laser) which falls well into the absorption maxima of **1a**–**1c** (Figure 3). All rR spectra reveal sets of modes characteristic for the coordinated terpyridine ligands which is evident when comparing with the rR data of the unsubstituted complex $[Ru(tpy)_2](PF_6)_2$ (Figure 3, Table 2).[13,34] Common to all ester complexes **1a**–**1c** is the resonance enhancement of a 1726 cm^{-1} mode which is easily assigned to the carbonyl stretching vibration of the ester groups (Figure 3).[18] In the off-resonance Raman spectrum of the tpy–$COOC_2H_5$ ligand in the solid state this vibration is observed at 1721 cm^{-1} (Supporting Information). Thus the ^{1}MLCT excited state is clearly associated with the electron-accepting tpy–$COOC_2H_5$ ligand as expected.[26]

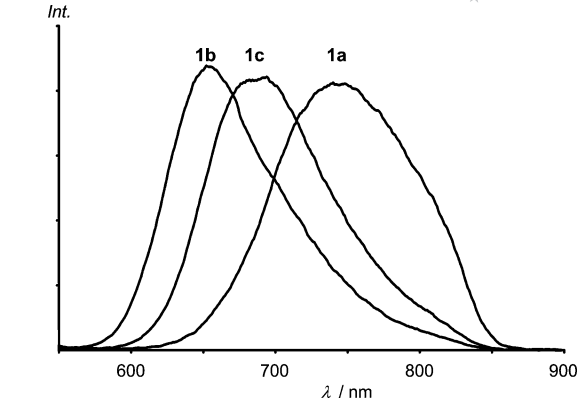

Figure 2. Emission spectra of **1a**–**1c** in CH_3CN at room temperature.

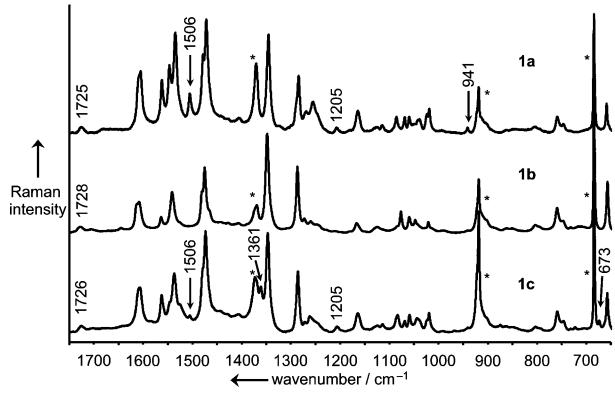

Figure 3. Resonance Raman spectra of **1a**–**1c** in CH_3CN with λ_{exc} = 488 nm (solvent bands are marked with asterisks).

Compared to the homoleptic complex **1b** some bands are split in the heteroleptic complexes **1a** and **1c** ($\tilde{\nu}$ = 1542, 1123, 1077, 1047, 1021 cm^{-1}). For **1a** and **1c** additional bands can be identified at 1205 cm^{-1} and 1506 cm^{-1} while the signal at 941 cm^{-1} is specific for **1a** (Table 2). The resonance enhancement of the 941 cm^{-1} mode is unique to the amine complex **1a** and thus probably associated with the NH_2-substituted ligand. Unfortunately, the off-resonance Raman spectra of the ligands tpy–$COOC_2H_5$ and tpy–NH_2 (see Supporting Information) are of little help in assigning

Table 2. Raman data of $[Ru(tpy)_2](PF_6)_2$ and **1a**–**1c** in CH_3CN at room temperature.

$[Ru(tpy)_2](PF_6)_2$ λ_{exc} = 458 nm	**1a** λ_{exc} = 488 nm	**1b** λ_{exc} = 488 nm	**1c** λ_{exc} = 488 nm
	1725	1728	1726
1602	1608 (sh), 1606	1612 (sh), 1609	1607 (br)
1559 (sh)	1563	1564	1563
1549	1547, 1536	1542	1546 (sh), 1538
	1506		1506
1490	1479	1480	1479 (sh)
1470	1473	1476	1474
1328	1347	1349	1361, 1348
1284	1285, 1269, 1255	1288, 1273, 1260	1287, 1271, 1260
1183	1205		1205
1164	1164	1165	1164
1101	1125, 1114	1123	1123, 1113
1094	1085, 1069, 1059, 1042, 1038	1077, 1060, 1047	1083, 1069, 1059, 1042, 1038 (sh)
1018	1023, 1019	1021	1022 (sh), 1020
	941		
748	759, 746	760, 746	759, 745
718			
673	685, 659	685, 657	685, 673, 658

individual bands in the fingerprint region. This might be due to the different conformation of the terpyridine unit in the free ligand (*transoid*), while coordination to the metal center enforces a *cisoid* conformation.

These observations indicate that upon excitation with λ_{exc} = 488 nm the ^{1}MLCT transitions are associated both with the tpy–$COOC_2H_5$ *and* the tpy–NHX ligand in **1a** (X = H) and **1c** (X = $COCH_3$).

In a molecular orbital picture the π* orbital of tpy–NH_2 should be higher in energy than that of tpy–$COOC_2H_5$ due to the electron-donating effect of the NH_2 group. Thus it would be anticipated that upon increasing the excitation energy (from λ_{exc} = 514 nm to λ_{exc} = 458 nm) resonance enhancement of tpy–NH_2 associated bands for **1a** should increase due to population of the π* orbital of tpy–NH_2. However, the contrary is observed (Figure 4). The unique

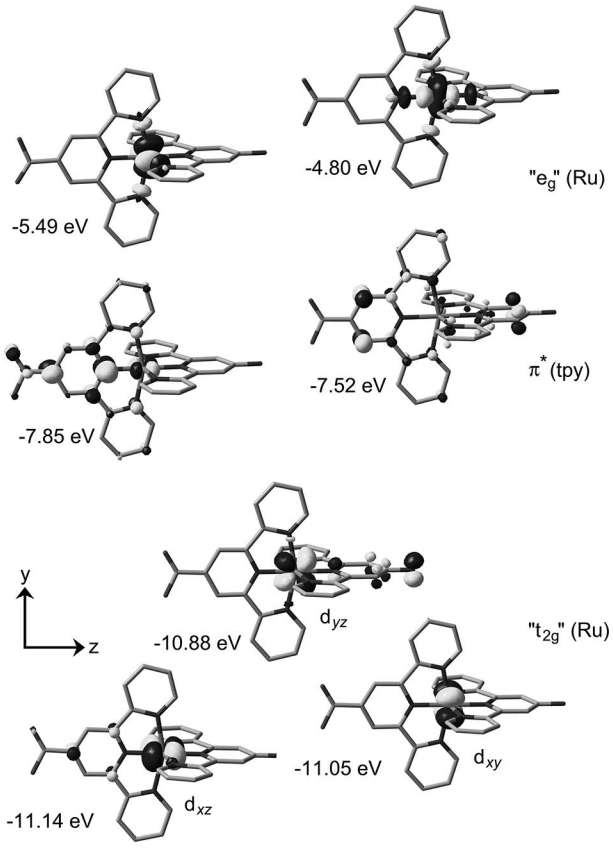

Figure 5. Relevant Kohn–Sham frontier orbitals of the model of amine complex **1a** (hydrogen atoms omitted for clarity, isosurface value 0.06 au).

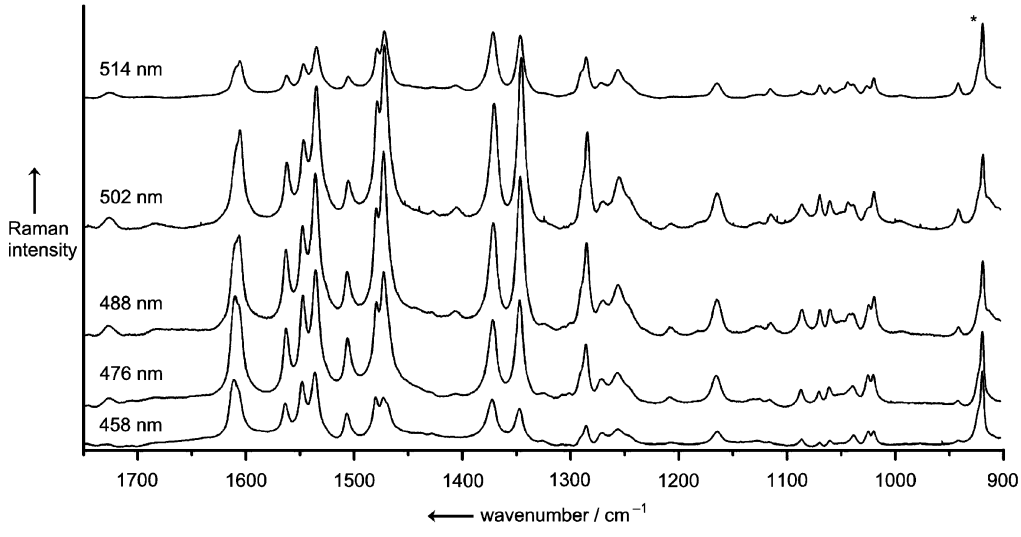

Figure 4. Resonance Raman spectra of **1a** in CH_3CN with λ_{exc} = 458, 476, 488, 502 and 514 nm (normalized to the solvent band at 919 cm^{-1}).

941 cm^{-1} mode of **1a** is more strongly resonance enhanced at *lower* excitation energies (Figure 4). The same trend of resonance enhancement is also clearly observed for bands at 1043, 1114 and 1605 cm^{-1} which are also associated with *N*-substituted terpyridine ligands (Table 2, Figure 4). As not only the π* acceptor orbitals (formally populated in the excited state) determine the resonance enhancement of vibrational modes but also the donor orbitals (formally depopulated in the excited state), relevant molecular orbitals of simplified models of the dications of **1a**–**1c** were calculated by DFT methods (see Figures 5, 6, and 7).[32,35]

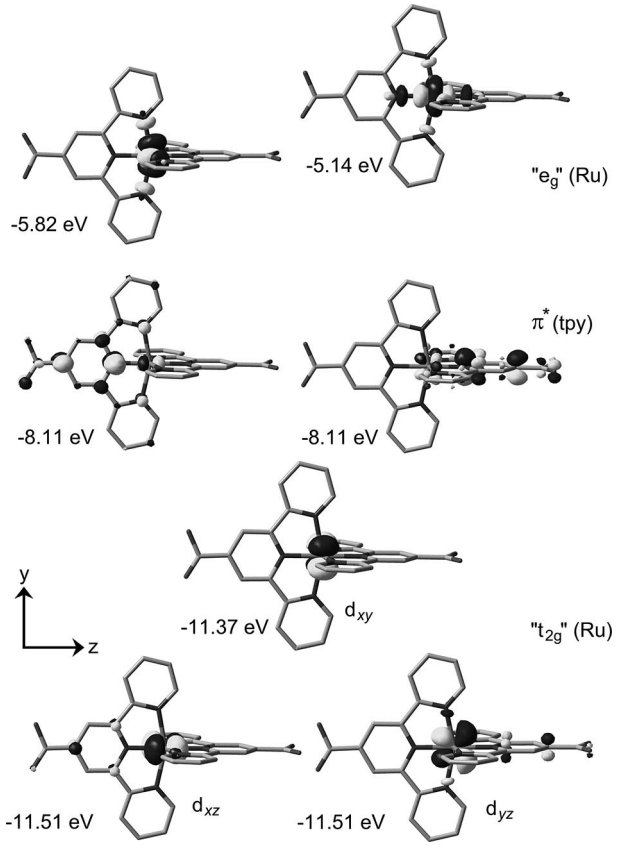

Figure 6. Relevant Kohn–Sham frontier orbitals of the model of diester complex **1b** (hydrogen atoms omitted for clarity, isosurface value 0.06 au).

As expected, the lowest unoccupied (acceptor) orbital of all complexes **1a**–**1c** is a π* orbital of tpy–$COOC_2H_5$ (Figures 5, 6, and 7). The π* orbitals of tpy–NH_2 and tpy–$NHCOCH_3$ in **1a** and **1c** are calculated to be about 0.3 eV higher in energy (Figures 5 and 7). The highest occupied (donor) molecular orbitals of all complexes **1a**–**1c** are the ruthenium-based d_{yz}, d_{xy} and d_{xz} orbitals (constituting the t_{2g} manifold in ideal O_h symmetry). However, it is also observed that the highest occupied molecular orbital of **1a** is a (Ru–N antibonding) mixture of the ruthenium-based d_{yz} orbital and an occupied π orbital of the tpy–NH_2 ligand (Figure 5). This composite orbital is separated by 0.17 eV and 0.26 eV from the other two metal-based occupied d_{xy} and d_{xz} orbitals (Figure 5). For **1b** and **1c** the degeneracy of the "t_{2g}" orbitals is much less lifted; the energy differences

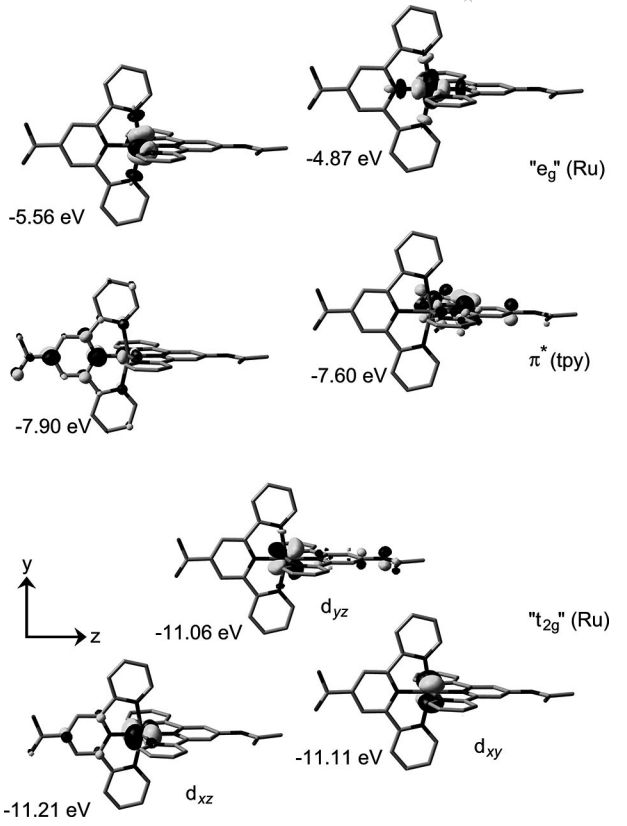

Figure 7. Relevant Kohn–Sham frontier orbitals of the model of amide complex **1c** (hydrogen atoms omitted for clarity, isosurface value 0.06 au).

between the highest d orbital and the other two d orbitals amount to only 0.14 eV/0.14 eV (**1b**) and 0.05 eV/0.15 eV (**1c**), respectively (Figures 6 and 7). The strong π-donor character of the tpy–NH_2 ligand manifests itself also in a planar amine substituent (angular sum 360°) oriented coplanar with the pyridine ring (H–N–C–C torsion angle –0.05°), a shorter C–N(substituent) bond (**1a**: 1.369 Å; **1c**: 1.400 Å) and a larger Ru–N(tpy–NHX) distance (**1a**: 2.023 Å; **1c**: 2.018 Å). Reciprocally, the *trans* Ru–N(tpy–$COOC_2H_5$) distance decreases from **1b** (2.007 Å) to **1c** (2.001 Å) to **1a** (1.998 Å) (Scheme 3). The π-donor character of the tpy–NH_2 ligand is best illustrated by the resonance structures of **1a** in Scheme 3 (bottom).

Thus it is proposed that the lowest energy excited singlet state of **1a** can be described by a $^1[\{d_{yz}/\pi(tpy–NH_2)\}^2] \rightarrow {}^1[\{d_{yz}/\pi(tpy–NH_2)\}^1\{\pi^*(tpy–COOC_2H_5)\}^1]$ designation. Obviously, this MLCT state possesses a significant ligand-to-ligand charge transfer (LLCT) $\pi(tpy–NH_2) \rightarrow \pi^*(tpy–COOC_2H_5)$ contribution while higher energy ^{1}MLCT states involve almost pure d_{xy} and d_{xz} metal donor orbitals. This interpretation is also in line with the observation that **1a** features the ^{1}MLCT absorption (λ_{max} = 500 nm) and ^{3}MLCT emission (λ_{max} = 744 nm) (both with the mentioned admixed LLCT character) with the lowest energies corresponding to the lowest HOMO/LUMO gap in the series described (Table 1). The small HOMO/LUMO gap of **1a** is also supported by the redox potentials of **1a**–**1c** which

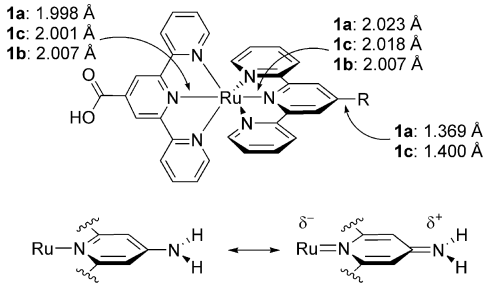

Scheme 3. Relevant DFT-calculated metrical parameters of models of **1a**–**1c** (top) and resonance structures of relevant parts of **1a** (bottom).

suggest a higher lying HOMO of **1a** (Table 1, Figure 5). In addition **1a** displays the highest lifetime τ of the emissive state (Table 1) which is probably also promoted by the admixed LLCT character. A red-shift of absorption and emission bands induced by admixed charge-transfer character has been previously observed in donor/acceptor-substituted porphyrin amino acids (*trans*-AB_2C disubstituted *meso*-porphyrins with A = C_6H_4–COOH, C = C_6H_4–NH_2 and B = C_6H_5).[36] Thus, the "destination" of the excited electron in complexes **1a**–**1c** is in all cases the π* orbital of the tpy–$COOC_2H_5$ ligand while the "origin" of the excited electron is different in **1a** [d_{yz},/π(tpy–NH_2) mixed orbital] as compared to **1b** and **1c** (mainly d orbitals). This interpretation is fully congruent with previously investigations on push-pull-substituted $[Ru(tpy–R)(tpy–R')]^{2+}$ (e.g. R = NMe_2, R′ = SO_2Me) complexes where it has been stated that the donor-substituted terpyridine ligand "destabilizes the metal centered π(t_{2g}) orbitals".[14]

Conclusions

Absorption, emission, and resonance Raman spectroscopy as well as electrochemistry and theoretical calculations support the view that the amino acid ester complex $[Ru(tpy–COOC_2H_5)(tpy–NH_2)]^{2+}$ (**1a**) is unique in the series described here. DFT calculations suggest that **1a** features a high-energy HOMO. The high energy HOMO results in a low Ru^{II}/Ru^{III} redox potential as well as red-shifted ^{1}CT absorption and ^{3}CT emission bands as expected from the electron pushing amine group. In parallel with the decreasing electron-donating effect of the substituents R = NH_2, $NHCOCH_3$, $COOC_2H_5$ the calculated HOMO/LUMO gap increases from 3.03 eV (**1a**) to 3.16 eV (**1c**) to 3.26 eV (**1b**).

The very strong π-donor character of the NH_2 group introduces π(tpy–NH_2) character into the HOMO of **1a** resulting in mixed MLCT/LLCT character of the excited states $^1[\{d_{yz}/\pi(tpy–NH_2)\}^1\{\pi^*(tpy–COOC_2H_5)\}^1]$ and $^3[\{d_{yz}/\pi(tpy–NH_2)\}^1\{\pi^*(tpy–COOC_2H_5)\}^1]$. This mixed MLCT/LLCT character might explain the resonance enhancement of tpy–NH_2 modes when excited at around 500 nm (singlet excited state) and the prolonged lifetime of the emitting triplet excited state. A less pronounced π(tpy–$NHCOCH_3$) participation in the HOMO and thus a less pronounced LLCT character for the MLCT states is suggested for the amide complex $[Ru(tpy–COOC_2H_5)(tpy–NHCOCH_3)]^{2+}$ (**1c**). Thus the admixed LLCT character of the MLCT states increases in the series **1b** < **1c** < **1a**. Whether this observation may be generalized and exploited for the design of photo-redoxactive metal complexes displaying prolonged excited state lifetimes will be subject of future work.

Experimental Section

General: Chemicals were obtained from commercial suppliers and used without further purification. Bis(terpyridine)ruthenium(II) complexes **1a** and **1b** were synthesized as reported.[18,25] Microwave accelerated reactions were conducted in heavy-walled glass vials sealed with aluminium crimp caps fitted with a silicone septum. The inner diameter of the vial that was filled to the height of 8 cm was 1 cm. Microwave heating was performed in a Discover Benchmate Plus (CEM Synthesis) single-mode microwave cavity producing continuous irradiation at 2.455 GHz with 100 W (max. power). Reaction mixtures were stirred with a magnetic stir bar during irradiation. Temperature and irradiation power were monitored during the course of the reaction. IR spectra were recorded on a BioRad Excalibur FTS 3000 spectrometer using caesium iodide disks. UV/Vis spectra were recorded on a Perkin–Elmer Lambda 19 in 1.0-cm cells (Hellma, suprasil). Mass spectra were recorded on a Finnigan MAT 8400 spectrometer. NMR spectra were obtained on a Bruker Avance DPX 200 (200 MHz, ^{1}H) at 30 °C. Chemical shifts (δ /ppm) are reported with respect to residual solvent peaks as internal standards: CD_3CN $\delta(^1H)$ = 1.94 ppm, $\delta(^{13}C)$ = 1.2, 117.7 ppm. Cyclic voltammetry was performed on a Metrohm "Universal Mess- und Titriergefaess", Metrohm GC electrode RDE 628, platinum electrode, SCE electrode, Princeton Applied Research potentiostat Model 273; in 0.1 M nBu_4NPF_6/CH_3CN. Potentials are given relative to that of SCE. Emission spectra were recorded on a Varian Cary Eclipse spectrometer. Quantum yields were determined by comparing the areas under the emission spectra on an energy scale [cm^{-1}] recorded for optically matched solutions of the samples and the reference $\{\phi([Ru(bpy)_3]^{2+}) = 0.062$ in $CH_3CN\}$;[31] experimental uncertainty 15%. Luminescence lifetimes were determined on a PicoQuant FluoTime 100 time-correlated single-photon counting unit. Lifetimes were extracted from the decay curve by an iterative reconvolution fitting routine with nonlinear error minimisation using the FluoFit Software. Criteria for the best fit were the values of χ^2; experimental uncertainty 10%. Resonance Raman spectra were measured with a conventional 90°-scattering arrangement. The excitation lines from 458 nm to 514 nm provided by an argon ion laser (Model Coherent Innova 300C MotoFreD Ion Laser) served for resonant excitation in the range of the MLCT absorption band. A rotating cell was utilized to prevent the heating of the samples. No changes in the absorption spectra could be observed after exposure to resonant laser light. The scattered light was collected with a lens ($f1$ = 35 mm) and subsequently focused ($f2$ = 50 mm) onto the entrance slit of an Acton SpectraPro 2758i spectrometer. The dispersed Raman stray light was detected with a CCD camera from Princeton Instruments, labeled with Spec-10 400B/LN back illuminated CCD. The concentration of the solutions was optimized to obtain a maximum signal-to-noise ratio and was in the millimolar range. Off-resonance Raman spectra were measured with a Horiba Jobin Yvon T64000 spectrometer with the 514 nm line of an argon ion laser operating at 300 mW. Density functional calculations were carried out with the Gaussian03/DFT[32] series of programs. The

B3LYP formulation of density functional theory was used employing the LANL2DZ basis set.[32] All structures were characterized as minima by frequency analysis (N_{imag} = 0). No symmetry constraints were imposed on the molecules. No solvent modeling was employed.

1c: **1a** (150 mg, 0.16 mmol) and acetic anhydride (24 mg, 0.24 mmol) were dissolved in CH_3CN (15 mL). Phosphazene base P_1-*t*Bu (27 mg, 0.98 mmol) was added and the mixture was heated to reflux for 2 h. After cooling the solvent was removed in vacuo. The residue was dissolved in ethanol and the product was precipitated by addition of NH_4PF_6 (78 mg, 0.48 mmol) in H_2O (1 mL). **1c** was obtained as a red powder (150 mg, 0.15 mmol, 94%). $C_{35}H_{29}N_7O_3RuP_2F_{12}$ (986.65)·$6H_2O$ calcd. C 37.78, H 3.89, N 8.81; found C 37.74, H 3.90, N 9.06. MS (FAB$^+$): *m*/*z* (%) = 842 (45) $[M+PF_6]^+$, 896 (100) $[M - H]^+$. IR (CsI): ṽ(tilde) = 3433 cm^{-1} (OH, NH), 3046 cm^{-1} (CH_{aryl}), 2936 cm^{-1} (CH_{alkyl}), 1717 cm^{-1} (C=O), 1683 cm^{-1} (Amide I), 1525 cm^{-1} (Amide II), 1563 cm^{-1} (C=N, C=C),1253 cm^{-1} (C–O), 874 cm^{-1} (PF). ^{1}H NMR (CD_3CN, 200 MHz): δ = 9.42 (s, 1 H, NH), 9.18 (s, 2 H, H^2), 8.96 (s, 2 H, H$^{2'}$), 8.65 (d, $^3J_{HH}$ = 8.0 Hz, 2 H, H^5), 8.38 (d, $^3J_{HH}$ = 8.0 Hz, 2 H, H$^{5'}$), 7.86–7.99 (m, 4 H, H$^{6,6'}$), 7.46 (d, $^3J_{HH}$ = 5.2 Hz, 2 H, H^8), 7.20–7.25 (m, 4 H, H$^{7,7'}$), 7.11 (ddd, $^3J_{HH}$ = 6.6, $^4J_{HH}$ = 1.20 Hz, 2 H, H$^{8'}$), 4.65 (q, $^3J_{HH}$ = 7.0 Hz, 2 H, CH_2), 2.37 (s, 3 H, H^9), 1.56 (t, $^3J_{HH}$ = 7. 1 Hz, 3 H, CH_3) ppm. ^{13}C NMR (CD_3CN, 50 MHz): δ = 171.5 (COOH), 165.0 (CONH), 158.6 (2 C), 158.0, 157.4 (C$^{3,3',4,4'}$), 153.7 (C$^{8'}$), 153.3 (C^8), 148.1 (C$^{1'}$), 137.0 (C^1), 139.2 (C$^{6'}$), 139.0 (C^6), 128.7 (C^7), 128.3 (C$^{7'}$), 125.7 (C^5), 125.3 (C$^{5'}$), 123.6 (C^2), 113.8 (C$^{2'}$), 63.7 (CH_2), 24.8 (C^9), 14.6 (CH_3) ppm. CV (CH_3CN, SCE, nBu$_4$NPF$_6$): 1.25 V (Ru^{II}/Ru^{III}), –1.15 V, –1.73 V (tpy/tpy$^-$).

Supporting Information (see also the footnote on the first page of this article): Cartesian coordinates of DFT optimized model structures of **1a**–**1c** and Raman spectra of the terpyrine ligands tpy–$COOC_2H_5$ and tpy–NH_2 in the solid state.

Acknowledgments

This work was supported by the Deutsche Forschungsgemeinschaft (DFG) (grant no. HE 2778/5-1).

[1] E. A. Medlycott, G. S. Hanan, *Coord. Chem. Rev.* **2006**, *250*, 1763–1783.
[2] J. G. Vos, J. M. Kelly, *Dalton Trans.* **2006**, 4869–4883.
[3] M. Grätzel, *Inorg. Chem.* **2005**, *44*, 6841–6851.
[4] F. Gao, Y. Wang, D. Shi, J. Zhang, M. Wang, X. Jing, R. Humphry-Baker, P. Wang, S. M. Zakeeruddin, M. Grätzel, *J. Am. Chem. Soc.* **2008**, *130*, 10720–10728.
[5] H. Hofmeier, U. S. Schubert, *Chem. Soc. Rev.* **2004**, *33*, 373–399.
[6] C. Siegers, J. Hohl-Ebinger, B. Zimmermann, U. Würfel, R. Mülhaupt, A. Hinsch, R. Haag, *ChemPhysChem* **2007**, *8*, 1548–1556.
[7] F. Felix, J. Ferguson, H. U. Güdel, A. Ludi, *J. Am. Chem. Soc.* **1980**, *102*, 4096–4102.
[8] M. I. J. Polson, F. Loiseau, S. Campagna, G. S. Hanan, *Chem. Commun.* **2006**, 1301–1303.
[9] M. I. J. Polson, E. A. Medlycott, G. S. Hanan, L. Mikelsons, N. J. Taylor, N. Watanabe, Y. Tanaka, F. Loiseau, R. Passalacqua, S. Campagna, *Chem. Eur. J.* **2004**, *10*, 3640–3648.
[10] R. Passalacqua, F. Loiseau, S. Campagna, Y.-Q. Fang, G. S. Hanan, *Angew. Chem.* **2003**, *115*, 1646–1649; *Angew. Chem. Int. Ed.* **2003**, *42*, 1608–1611.
[11] E. A. Medlycott, G. S. Hanan, *Chem. Soc. Rev.* **2005**, *34*, 133–142.
[12] a) J.-P. Sauvage, J.-P. Collin, J.-C. Chambron, S. Guillerez, C. Coudret, *Chem. Rev.* **1994**, *94*, 993–1019; b) J. R. Winkler, T. L. Netzel, C. Creutz, N. Sutin, *J. Am. Chem. Soc.* **1987**, *109*, 2381–2392; c) U. Siemeling, J. Vor der Brüggen, U. Vorfeld, B. Neumann, A. Stammler, H.-G. Stammler, A. Brockhinke, R. Plessow, P. Zanello, F. Laschi, F. Fabrizi de Biani, M. Fontani, S. Steenken, M. Stapper, G. Gurzadyan, *Chem. Eur. J.* **2003**, *9*, 2819–2833.
[13] A. A. Bhuiyan, J. R. Kincaid, *Inorg. Chem.* **1998**, *37*, 2525–2530.
[14] M. Maestri, N. Armaroli, V. Balzani, E. C. Constable, A. M. W. Cargill Thompson, *Inorg. Chem.* **1995**, *34*, 2759–2767.
[15] M. Abrahamsson, H. Wolpher, O. Johansson, J. Larsson, M. Kritikos, L. Eriksson, P.-O. Norrby, J. Bergquist, L. Sun, B. Åkermark, L. Hammerström, *Inorg. Chem.* **2005**, *44*, 3215–3225.
[16] H. J. Bolink, L. Capelli, E. Coronado, P. Gaviña, *Inorg. Chem.* **2005**, *44*, 5966–5968.
[17] U. S. Schubert, H. Hofmeier, G. R. Newkome, *Modern Terpyridine Chemistry*, Wiley-VCH, Weinheim **2006**.
[18] K. Heinze, K. Hempel, M. Beckmann, *Eur. J. Inorg. Chem.* **2006**, 2040–2050.
[19] K. J. Kise Jr., B. E. Bowler, *Inorg. Chem.* **2002**, *41*, 379–386.
[20] D. J. Hurley, J. R. Roppe, Y. Tor, *Chem. Commun.* **1999**, 993–994.
[21] B. M. Bishop, D. G. McCafferty, B. W. Erickson, *Tetrahedron* **2000**, *56*, 4629–4638.
[22] W. H. Soine, C. E. Guyer, F. F. Knapp Jr., *J. Med. Chem.* **1984**, *27*, 803–806.
[23] a) K. Heinze, M. Beckmann, K. Hempel, *Chem. Eur. J.* **2008**, *14*, 9468–9480; b) K. Heinze, K. Hempel, *Chem. Eur. J.* **2009**, *15*, 1346–1358.
[24] J. R. Kincaid, K. Czarnecki, *Resonance Raman: Coordination Compounds*, in: *Comprehensive Coordination Chemistry II* (Eds.: J. A. McCleverty, T. J. Meyer), vol. 2, Elsevier, Amsterdam, **2003**.
[25] M. H. Chisholm, C. M. Hadad, K. Heinze, K. Hempel, N. Singh, S. Vyas, *J. Cluster Sci.* **2008**, *19*, 209–218.
[26] M. Schwalbe, B. Schäfer, H. Görls, S. Rau, S. Tschierlei, M. Schmitt, J. Popp, G. Vaughan, W. Henry, J. G. Vos, *Eur. J. Inorg. Chem.* **2008**, 3310–3319.
[27] C. Herrmann, J. Neugebauer, M. Presselt, U. Uhlemann, M. Schmitt, S. Rau, J. Popp, M. Reiher, *J. Phys. Chem. B* **2007**, *111*, 6078–6087.
[28] S. Tschierlei, B. Dietzek, M. Karnahl, S. Rau, F. M. MacDonnell, M. Schmitt, J. Popp, *J. Raman Spectrosc.* **2008**, *39*, 557–559.
[29] M. K. Nazeerruddin, M. Grätzel, *Conversion and Storage of Solar Energy using Dye Sensitized Nanocrystalline TiO_2 Cells*, in: *Comprehensive Coordination Chemistry II* (Eds: J. A. McCleverty, T. J. Meyer), vol. 9, Elsevier, Amsterdam, **2003**.
[30] *Artificial Photosynthesis: From Basic Biology to Industrial Application* (Eds: A. F. Collings, C. Critchley), Wiley-VCH, Weinheim, **2005**.
[31] J. V. Caspar, T. J. Meyer, *J. Am. Chem. Soc.* **1983**, *105*, 5583–5590.
[32] *Gaussian 03, Revision B.03*, M. J. Frisch, G. W. Trucks, H. B. Schlegel, G. E. Scuseria, M. A. Robb, J. R. Cheeseman, J. A. Montgomery Jr., T. Vreven, K. N. Kudin, J. C. Burant, J. M. Millam, S. S. Iyengar, J. Tomasi, V. Barone, B. Mennucci, M. Cossi, G. Scalmani, N. Rega, G. A. Petersson, H. Nakatsuji, M. Hada, M. Ehara, K. Toyota, R. Fukuda, J. Hasegawa, M. Ishida, T. Nakajima, Y. Honda, O. Kitao, H. Nakai, M. Klene, X. Li, J. E. Knox, H. P. Hratchian, J. B. Cross, C. Adamo, J. Jaramillo, R. Gomperts, R. E. Stratmann, O. Yazyev, A. J. Austin, R. Cammi, C. Pomelli, J. W. Ochterski, P. Y. Ayala, K. Morokuma, G. A. Voth, P. Salvador, J. J. Dannenberg, V. G. Zakrzewski, S. Dapprich, A. D. Daniels, M. C. Strain, O. Farkas, D. K. Malick, A. D. Rabuck, K. Raghavachari, J. B.

Foresman, J. V. Ortiz, Q. Cui, A. G. Baboul, S. Clifford, J. Cioslowski, B. B. Stefanov, G. Liu, A. Liashenko, P. Piskorz, I. Komaromi, R. L. Martin, D. J. Fox, T. Keith, M. A. Al-Laham, C. Y. Peng, A. Nanayakkara, M. Challacombe, P. M. W. Gill, B. Johnson, W. Chen, M. W. Wong, C. Gonzalez, J. A. Pople, *Gaussian*, Inc., Pittsburgh PA, **2003**.

[33] E. M. Kober, T. J. Meyer, *Inorg. Chem.* **1982**, *21*, 3967–3977.

[34] B. J. Coe, D. W. Thompson, C. T. Culbertson, J. R. Schoonover, T. J. Meyer, *Inorg. Chem.* **1995**, *34*, 3385–3395.

[35] For simplification of the model and facilitating convergence of geometry optimisation algorithms the ethyl groups in **1a**–**1c** were replaced by hydrogen atoms, i.e. ethyl ester units are replaced by acid groups. In gas-phase calculations, i.e. without intermolecular interactions, this should leave the calculated frontier orbital energies and frontier orbital compositions rather unaffected.

[36] K. Heinze, A. Reinhart, *Dalton Trans.* **2008**, 469–480.

Received: April 2, 2009
Published Online: June 5, 2009

